# Characterization of abnormal lubricant film pressure distribution mechanisms in pure sliding AISI52100 ball bearing contacts using sliding contact fatigue distribution and wear behaviour

*Sipho* Masilela[1*], *Charles* Siyasiya[2], and *Roelf* Mostert[3]

[1]Measurement and Control Department, Mintek, Randburg 2125, South Africa
[1,2,]Department of Materials Science and Metallurgical Engineering, University of Pretoria, Hatfield 0083, South Africa

**Abstract.** Ball bearings are a critical component of transmission systems whose operation depends on efficient lubrication. Moving surfaces in ball bearings are typically manufactured from AISI52100 martensitic steel material. During operation, a critical role of the lubricant is to generate film-pressure, which creates film thickness and separates the moving surfaces. There is lack of knowledge regarding abnormal film-pressure generating mechanisms occurring in ball bearings during pure sliding motions. In this study, sliding contact fatigue and wear behaviour are used to characterise abnormal film-pressure distribution behaviours, which reveal the appearance of abnormal film pressure generating mechanisms in pure sliding AISI5200 ball bearing contacts. A set of pure sliding experiments were conducted using a wear test machine with a ball bearing configuration. Abnormal plastic deformation and wear behaviour on the worm bearing surfaces indicate the appearance of an abnormal collaboration between two film pressure generating mechanisms i.e., the viscosity wedge effect (VWE) and the squeeze effect. The VWE is described where abnormal surface deformation is observed, and the squeeze effect, where deformation is influenced by the change in sliding speed. These findings reveal, for the first time, the domain of action of each effect in the ball bearing contact area.

## 1 Introduction

Ball bearings are critical components in transmission systems in automotives, whose operation depends on efficient lubrication. Moving surfaces of ball bearings are typically manufactured from AISI52100 martensitic steel material [1]. During operation, a critical role of the lubricant is to build film-pressure within itself, which increases the film thickness that separates the moving surfaces. To achieve this task, different lubricants employ different

* Corresponding author: u28411341@tuks.co.za

mechanisms, which are governed by one or more fluid flow phenomena. Published research shows that under pure sliding motions at high speeds, the build-up of film-pressure, is achieved through a collaboration between two effects i.e., a thermal effect called the viscosity wedge effect (VWE) and a mechanical effect called the squeeze effect [2, 3]. By definition, the VWE is a film-pressure generating effect caused by changes in viscosity, due to changes in temperature within a lubricant film, in the entrainment direction [4, 5]. The temperature changes cause large temperature gradients in the proximity, which induce viscosity and velocity gradients, which then cause the pressure gradients within the lubricant film. The squeeze effect is defined as the rate of change of film-thickness in a bearing due to dynamic (non-steady state) operating conditions [2, 3]. Non-steady state conditions involve dynamic loads and speeds, as well as significant surface deformation which the changes in the radius of curvature of lubricated surfaces. Such conditions are typical in ball bearings [6] and cause a continuous change in the volume of lubricant entrained into the contact area, which results in a continuous change of film-thickness, which indicates a rate of film-pressure generation. As such, the squeeze effect is inevitable in ball bearings, and it is, therefore, a default mechanism. In literature published thus far, the appearance of the collaboration between the VWE and squeeze effect has been studied using optical interferometry methods (see Fig. 1), and has been found to cause the appearance of abnormal film shapes in the ball bearing contact area. Abnormal film shapes exhibit a horse-shoe shape, with a side profile showing a dimple shaped central plateau, and an exaggerated outlet constriction (see Fig. 2). The dimple-shaped central plateau indicates the appearance of the dimple phenomenon in the leading-edge of the contact area. The dimple phenomenon has been accepted as a characteristic attribute of abnormal film shapes, which are associated to the appearance of the VWE [7, 8].

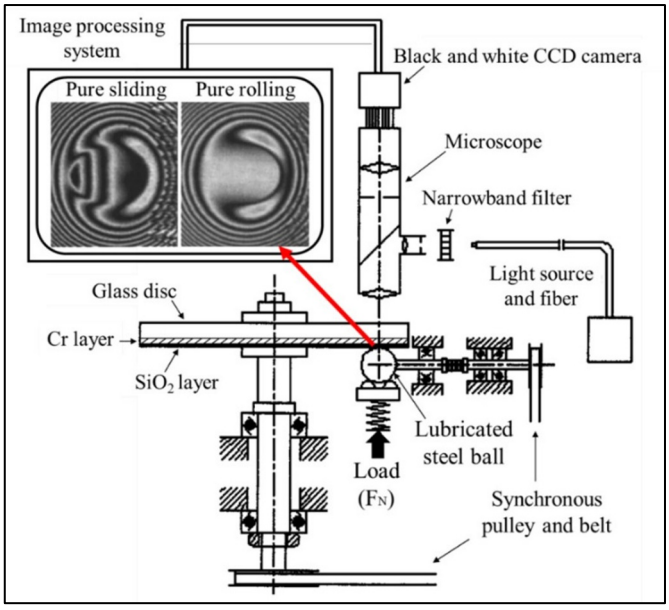


**Fig. 1.** Typical optical interferometry test apparatus (adapted from refs. [7, 9]).

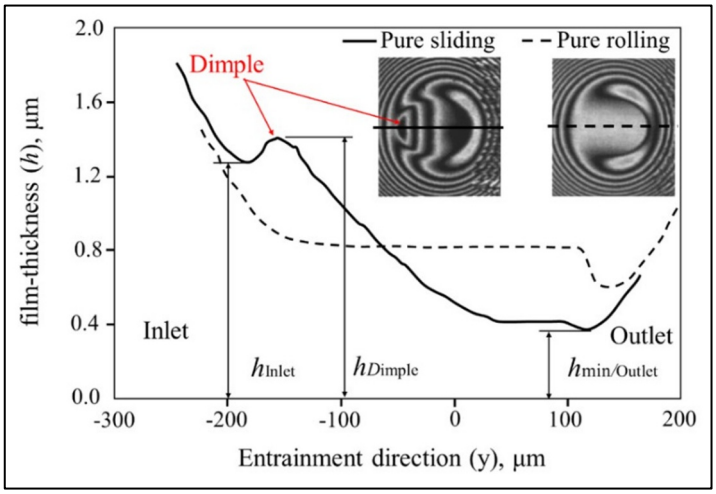


**Fig. 2.** Comparison of an abnormal (pure sliding) ball bearing film-thickness profile, with the classical (pure rolling) ball bearing film-thickness profile. h – height of lubricant film (adapted from ref. [7]).

The appearance of abnormal film shapes has also been found to be accompanied by solidification of the lubricant [10], as well as the interfacial slip phenomenon [10-12], which indicate non-Newtonian behaviour by the lubricant. Due to this, conventional lubrication theory, which is derived on the basis on the Newtonian behaviour of the lubricant, cannot predict the appearance of abnormal film shapes. Conventional lubrication theory predicts a film distribution profile with a horse-shoe shape, however, with a side profile showing a flat central plateau and a small constriction at the exit (see Fig. 2). This is regarded as the conventional (normal) film shape in ball bearings, and it is governed solely by the squeeze effect. This film shape is typical in pure rolling contacts or under low slide-roll ratios, where thermal effects are low [7]. Although optical interferometry has enabled significant progress in the study of film shapes and film pressure generation in ball bearing contacts, it has its limitations. The requirement of a transparent material in optical interferometry limits the experimentation, and the evidence obtained, to contacts between dissimilar materials (i.e., steel ball sliding on a chromium coated glass disc). Due to this limitation, there is a lack of knowledge regarding the appearance and effects of the VWE and squeeze effect in industrial ball bearing contacts which use similar sliding materials. This is specifically referring to ball bearings manufactured from the martensitic AISI52100 steel material, since this type of steel is a common choice of material for automotive and industrial ball bearings. This necessitates an investigation which will close this knowledge gap, and as such, this forms a basis for the current investigation. The aim of this investigation is to demonstrate and characterise, for the first time, the appearance and the effects of the abnormal film-pressure distribution behaviour caused by the collaboration between the VWE and the squeeze effect in pure sliding AISI5200 ball bearing contacts, under controlled laboratory conditions. This is achieved through assessment of sliding contact fatigue behaviour, and the wear behaviour, on the ball bearing surfaces. Experimental conditions for the ball bearing operation were selected to ensure the occurrence of sliding contact fatigue and wear on the sliding surfaces of the bearing. Results from this investigation provide experimental evidence for an extension of lubrication theory, which is required to advance bearing designs and the modelling and prediction of film-pressure distribution, surface deformation and wear behaviour in ball

bearing contacts. Furthermore, since martensitic type steel balls are used as grinding media in grinding mills in the mineral processing sector, the knowledge from this study enables advancement in the modelling and prediction grinding media wear and shear energy distribution in ball mills.

## 2 Experimental details

### 2.1 Materials and testing machine

The SRV4 wear test machine, with an oscillatory sliding ball on a stationery disc configuration, was used (SRV4, Optimol Instruments, Germany). The test chamber of the machine is shown in Fig. 3. The ball and disc specimens were purchased from Optimol Instruments, are AISI52100 bearing steel material, with a Vickers hardness of 600 HV, bulk modulus of 140 GPa, modulus of elasticity of 210 GPa, shear modulus of 80 GPa and thermal conductivity of 46.6 W/mK. The ball specimens are 10 mm in diameter, with a polished surface with roughness of 0.025 µm (Ra). The disc specimen has a 24 mm diameter and 7.9 mm height, and a lapped surface with roughness ranging between 0.45 to 0.65 µm (Rz). A commercial hydroprocessed Group III base oil, with a 100 °C kinematic viscosity ($KV_{100°C}$) of 4 cSt, was selected as a lubricant for the experiments. The classification (grouping) of the selected lubricant is based on its method of production, as per the American petroleum institute (API) [13, 14]. Table 1 lists the respective rheological properties. The rheological properties were measured at atmospheric pressure, using a Stabinger Viscometer (SVM 3001, Anton Paar GmbH, Austria). The lubricant is a neat hydrocarbon (contains no additive package) and is produced by hydroprocessing of crude oil with mild hydrocracking. The producer (supplier) cannot be disclosed (protected by non-disclosure agreement), however, the method of production was made known and permission for chemical analysis was given.

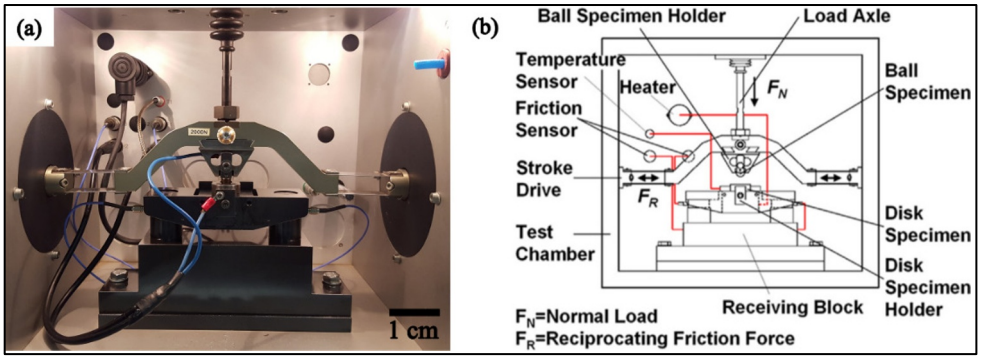


**Fig. 3.** Oscillatory sliding wear test machine. (a) Camera image, (b) detailed schematic.

**Table 1.** Lubricant selection and respective rheological properties.

| Lubricant ID | $KV_{100°C}$ (cSt) | $\rho_{25°C}$ (g/cm³) | $DV_{25°C}$ (mPa.s) | $SR_{25°C}$ (1/s) | $SS_{25°C}$ (Pa) | VI (-) |
|---|---|---|---|---|---|---|
| G3 S2 | 4.33 | 0.83 | 30.55 | 271.99 | 8.31 | 127.91 |

S2 – Supplier 2, ρ – density, DV – dynamic viscosity, SR - Shear Rate, SS - Shear Stress

### 2.2 Experimental procedure

The experiment was conducted for 2 hours, at 25 ± 0.5 °C and 20 ± 5 % relative humidity (RH). The controlled humidity atmosphere was to diminish the effect of atmospheric water on the wear process. The effect of atmospheric water is demonstrated by [15]. The sliding speed was set at 0.2 $m.s^{-1}$. This was achieved by setting a stroke length of 2 mm and oscillating frequency of 50 Hz. Due to the oscillatory motion, the sliding speed is not constant. The speed is maximum (0.2 $m.s^{-1}$) at the mid-stroke position (i.e., at mid-length, based on the sliding length on the flat surface), and reaches a minimum at full-stroke, where change in sliding direction occurs. There are two load stages to the experiments. The first stage is the run-in stage, where the normal load ($F_N$) is held at 30 N for 30 s. This is followed by a 30 s gradual load increase (at 4 $N.s^{-1}$) to a final load of 150 N. The normal load is kept constant at 150 N for the remainder of the test duration. The normal load is applied vertically on the ball specimen through a programmable spring loading system, and the sliding speed is achieved by application of a horizontal reciprocating sliding force ($F_R$). Both the normal load and oscillating speed are maintained through a programmable feedback system.

The steel specimens were cleaned by submerging in hexane, followed by acetone, under ultrasonic vibration for 10 minutes each using an ultrasonic bath. Specimens were oven dried at 90 °C for 5 minutes after ultrasonication. Cooling was conducted in a desiccator containing silica ($SiO_2$) granules. After assembling, 2 mL of lubricant was injected onto the flat surface before the ball was allowed to make contact, and the test chamber was conditioned at 25 °C for 10 minutes prior to the start of the experiment. After the sliding experiment, specimens were ultrasonically cleaned in hexane and acetone. Optical micrographs of worn surfaces were analysed using a Zeiss axio scope A1 optical microscope (Carl Zeiss microscopy GmbH, Germany). To obtain the physical details of the worn surfaces, 3-dimensional (3D) surface profiles were generated using a Nanovea PS50 optical profilometer (Nanovea Instruments Inc., USA).

## 3 Results and discussions

### 3.1 Surface deformation and film-pressure distribution

Optical microscope images in Fig. 4 shows the appearance of the Hertzian zones on the ball and flat surface. The Hertzian zone on the ball is slightly larger, in diameter (445 μm), than that of the flat surface (431 μm). This is due to the elastic deformation of the ball which was pressed against the flat surface by the Hertzian pressure. The ball surface shows a grey surface colour distribution across the center on the Hertzian zone, perpendicular to the sliding direction, and a mixture of blue and red surface colours are distributed at the top and bottom edges. On the flat surface, the grey colour is dominant in the center of the Hertzian zone, in the sliding direction, and the blue colour dominates the side edges, with small patches of red. The appearance of surface colours indicates oxidational wear. However, the colour distribution is unusual and appears to be caused by the appearance of abnormal contact conditions during the sliding process. To begin uncovering these abnormal contact conditions, the deformation behaviour is analysed through 3D analysis.

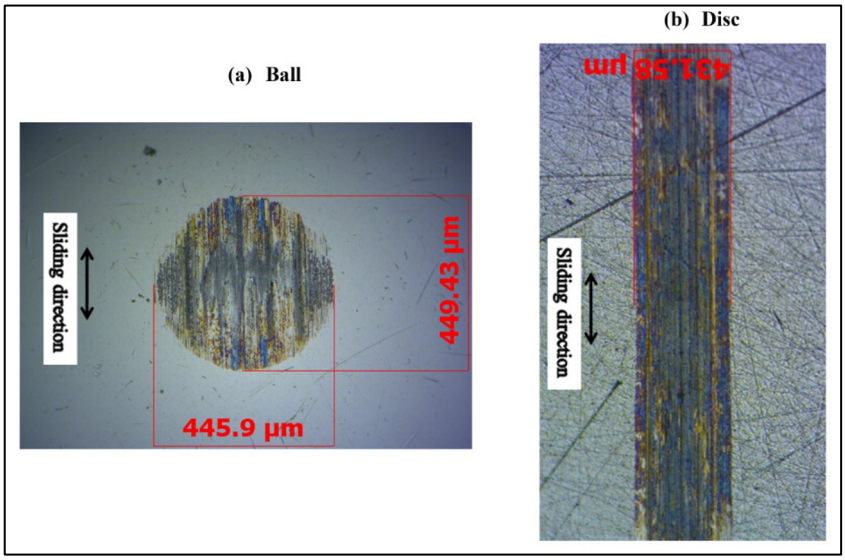


**Fig. 4.** Optical properties of worn ball and flat surfaces.

Fig. 5 shows the 3D surface profiles of the deformed surfaces. The 3D profile of the flat surface shows permanent indentations on the side-edges of the Hertzian zone. The indentations are deeper at the top and bottom tips. The increase in width and depth of the indentations at the tips of the side edges is associated to the decrease in sliding speed during change of sliding direction. From the depth profiles, the depth at maximum sliding speed (mid-stroke depth) is approximately 1 µm, and depth at minimum sliding speed (depth at the tips) is approximately 1.5 µm. This deformation behaviour indicates that the Hertzian pressure was carried by the side edges during the sliding process. The middle section shows essentially no deformation, indicated by presence of prominent surface roughness across the length of the Hertzian zone. This indicates minimal Hertzian pressure in the middle section, and no visible effect of the change in sliding speed. The sporadic presence of indents in the middle section is associated to the breaking of prominent surface asperities by shear stress resulting from the oscillatory sliding action. In the area marked "GWE", the indentation and widening of the approximately 1.5 µm deep scratch (which was present before the onset of sliding as a surface defect) is associated with the appearance of the geometry wedge effect (GWE), which causes the VWE on the flat surface due to surface defects, as was observed by [16]. This effect is discussed in later works by the authors of this work. The 3D profile of the ball shows significant deformation around the edges of the Hertzian zone, i.e., the leading edge and side edges, and minimal deformation in the center of the Hertzian zone. This indicates that the Hertzian pressure was maximum in the edges, and was minimal at the center, during the sliding process. Therefore, the Hertzian zone can be partitioned into three regions, i.e., leading-edge, center (outlet), and side-edges. Similarly with the flat surface, the side-edges, top and bottom edges, and middle section.

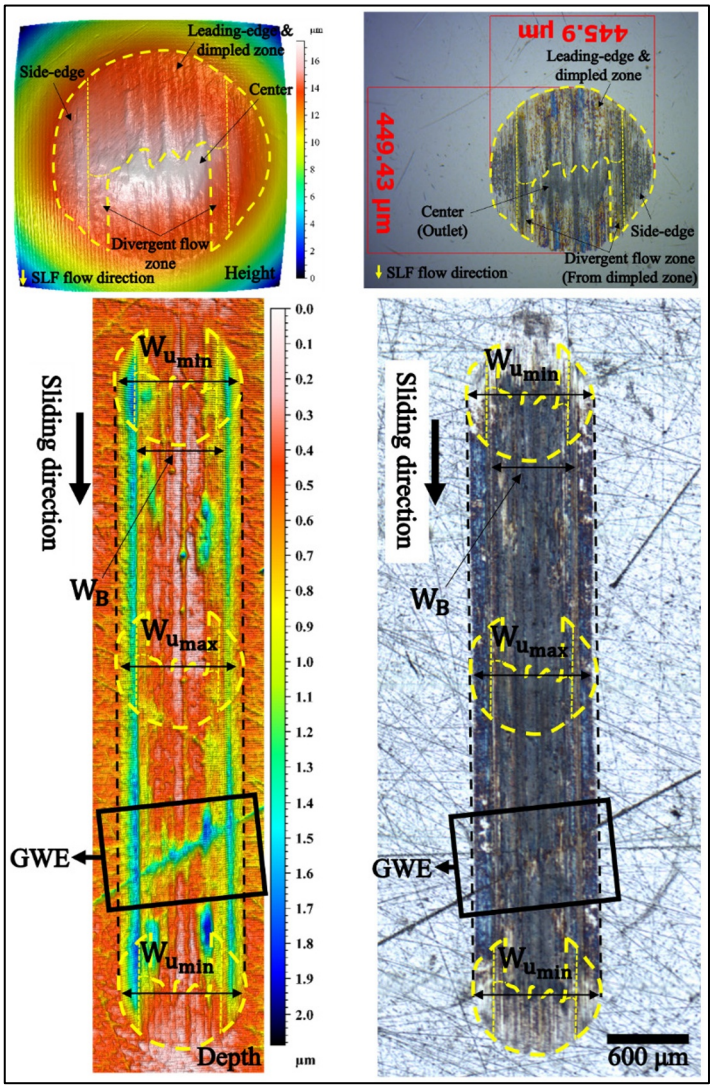


**Fig. 5.** Post sliding surface topography of ball and flat surfaces. **SLF** - Solid lubricant flow. $\mathbf{W_{u_{max}}}$ - width at maximum speed. $\mathbf{W_{u<u_{max}}}$ - width at minimum speed. $\mathbf{W_B}$ - width of middle section. **GWE** – Geometry wedge effect.

The transfer of Hertzian pressure between the ball and flat surface occurs through the lubricant film. Therefore, the distribution of Hertzian pressure in the Hertzian zone is controlled by the lubricants flow behaviour. The lubricant carries the Hertzian pressure, which acts vertically on the ball surface, by generating film pressure within itself, around the edges of the ball Hertzian zone. The build-up of film pressure enables the transmission of Hertzian pressure from the deformed ball-lubricant interfaces, through the high-pressure lubricant film, and to the side edges on the flat surface. Likewise, the high film pressure enables the backwards transmission of the reaction pressure exerted by the flat surface, to the ball. The reaction pressure is the pressure that indirectly supports the Hertzian pressure. A schematic of the reaction pressure is shown in Fig. 8, which is discussed in later sections of

this work. Therefore, during the sliding process, each surface interacts and reacts to the film pressure generated by the lubricant at the deformed metal-to-lubricants interfaces, which implies that the film pressure was maximum at the deformed regions. The observed deformation is caused by the repetitive action of the lubricant film pressure on the steel surfaces, during each of the approximately 360000 sliding cycles. From the flat surface, it is clear that the film pressure was distributed sideways to the side edges. However, the deformation on the ball is quite complex, especially with maximum deformation being in the leading edge (dimpled zone). This indicates that the film pressure distribution mechanism which supports and transfers the Hertzian pressure from the ball surface to the flat surface is complex, and requires thorough probing. Fig. 6 shows a flattened 3D height profile of the ball.

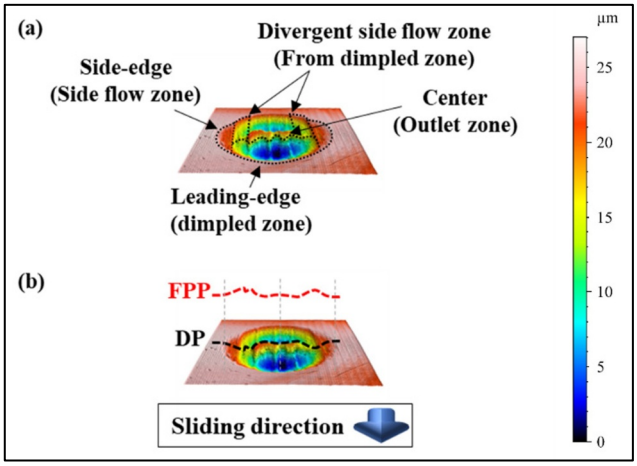


**Fig. 6.** Flattened 3D height profile of deformed ball and extrapolation of abnormal Hertzian pressure distribution in a point contact. FPP – Film pressure profile. DP – Depth profile.

By flattening the profile, a severe condition of both elastic and plastic deformation can be illustrated, and since surface deformation is caused by the lubricant film pressure, where Hertzian-pressure is carried, the shape of the film-pressure distribution profile can be extrapolated. Therefore, a depth profile (DP) is obtained across the center, perpendicular to the sliding direction, as illustrated by the dotted black line, and the shape of the film-pressure distribution profiles (FPP) is obtained by taking the inverse of the depth profiles (i.e., FPP = 1/DP), as illustrated by the dotted red line. The shape of the FPP shows two peaks, with each peak positioned on each side-edge, and goes through a minimum near the center. The film-pressure distribution profile has the shape of a fourth-degree polynomial. This indicates a sideways film-pressure distribution behaviour across the center of the Hertzian zone and perpendicular to the sliding direction. The flattened ball profile shows significant dimple shaped deformation in the leading-edge, indicating that film pressure is the highest in the leading edge. In the sliding direction, the dimple shaped deformation creates an exaggerated constriction which appears to constrict the flow of the lubricant towards the center of the Hertzian zone. This deformation behaviour indicates the appearance of the inlet dimple phenomenon, which is characteristic of abnormal film shapes and indicates appearance of the VWE [7, 8]. This deformation behaviour shows that the film pressure distribution has a horseshoe shape, and the pressure peaks in the leading edge. This film pressure distribution is abnormal, since pressure is expected to be maximum at the center of the Hertzian zone on both the ball and flat surface, because by convention in Hertzian (point) contacts, the Hertzian

pressure and film pressure are maximum at the center, and minimum at the edges of the Hertzian zone [17, 18]. This indicates that the film pressure generated by the VWE in the leading-edge is larger than that caused by the side flows. Therefore, the VWE carried a largest magnitude of the Hertzian pressure in the bearing, during the sliding process. The lubricant generated a high enough film pressure to induce plastic deformation in the permanently deformed edges of the Hertzian zone. This finding suggests that in the deformed regions of the Hertzian zone, the film-pressure, which also acts as shear stress, exceeded the yield stress of the steel material [1] and resulted in plastic flow of surface material [19]. Plastic flow is a form of shear stress induced material failure or fatigue mechanism, which leads to the observed permanent (plastic) deformation on the surface [19]. For the AISI52100 steel material with a Vickers hardness of 600 HV, this suggests that the lubricant must be in a solid state to induce plastic deformation on the steel surfaces. Solidification of the lubricant occurs when the local film pressure exceeds the glass transition pressure of the lubricant as was observed by [10]. In the solid state, the lubricant is immobile, and shears like an elastic amorphous solid with a yield strength [20].

## 3.2 Analysis of lubricant flow behaviour

In the previous section, it was established that the lubricant must be in a solid state to induce plastic deformation on the steel surfaces. Therefore, in Fig. 4, based on the plastic deformation behaviour on the ball surface, the shape of the solidified portion of the lubricant film is extrapolated, as illustrated in yellow. The solidified lubricant film (SLF) has a horseshoe shape. The SLF shape is then superimposed over the Hertzian zone of the flat surface, for the downwards sliding motion, at three positions i.e., top edge, mid-stroke, and bottom edge, respectively.

### *3.2.1 Role of the viscosity wedge effect*

The superimposed SLF shape shows that the leading-edge of the ball Hertzian zone is positioned directly above the middle section of the flat Hertzian zone. This indicates that solid-to-solid contact conditions occurred only in the leading-edge on the ball surface, while on the flat surface, which lies directly beneath, fluid-to-solid contact conditions occurred. This also indicates that the film-pressure, as well as viscosity of the lubricant, varied significantly across the film-thickness (height), since the lubricant was in a solid state at the ball-lubricant interface and was in the fluid state on the disc-lubricant interface. This behaviour is associated to the action of the VWE in the leading-edge. From the microscope image in Fig. 4, the center of the ball Hertzian zone shows a grey surface colour similar to that observed in the middle section of the flat surface. This is associated to fluid-to-solid contact conditions. This indicates a negative viscosity gradient at the lubricant-ball surface, between the leading-edge and the center. Between the center of the ball surface and the middle section of the flat surface, the lubricant was in a fluid state and this indicates the absence of a significant pressure and viscosity gradient across the film-thickness (height) in this region. Therefore, the VWE is trivial in this region. The side-edges of both the ball and flat surfaces show attributes of solid-to-solid contact conditions. This suggests complete solidification across the film-thickness, and also indicates a more direct transfer of the Hertzian pressure from the ball, through the solid lubricant film, to the flat surface.

It appears that the high pressure created by the VWE creates a flow stagnation zone in the leading-edge, which carries the Hertzian pressure (normal load) but also causes the sideways divergence of the incoming lubricant flow. The diverted flows combine with direct in-flows

in the side-edges, and this increases the volume of lubricant in the side-edges, and reduces the volume of lubricant reaching the center. This sideways flow diversion was also observed by Tošić et al. [21], where a strong VWE was thought to be responsible for the diversion of lubricant flow to the contact sides, which limited the volume of fluid lubricant maintaining the film in the central region of the Hertzian zone. The increase in volume in the side-edges causes flow constrictions, which generate positive film-pressure which forces an increase in film thickness. In this way, the load carrying capacity of the side edges increases. Since the sliding speed is not constant, the increase in film thickness occurs at a rate that changes with the sliding speed. This indicates a rate of change of film-pressure generation, which defines the appearance of the squeeze effect in the side edges [2]. The build-up of film-thickness (squeeze effect) competes with the compressive Hertzian pressure from the ball surface, which increases the constrictions, the viscosity and the pressure within the fluid film. The film pressure increases such that the glass transition pressure ($P_g$) of the lubricant is reached, and as such, glass transition (solidification) is induced [20]. This causes appearance of solid-to-solid contact conditions, which allow direct Hertzian pressure transfer through the solidified film, and also causes plastic deformation on both surfaces when the film-pressure, and its resulting shear stress, exceeds fatigue stress limit (yield stress) of the surface. Most importantly, the solid lubricant film barricades the side-edges, which prevents side leakages or the lubricant being pumped out of the Hertzian zone. As a result, the film-thickness and mass conservation are conserved in the Hertzian zone. This behaviour also depressurizes the center of the ball and middle section of the flat surface, and as such, the lubricant retains its fluidity in this region. It appears that the mechanism employed by the lubricant to separate of the sliding surfaces is such that the Hertzian pressure is first carried in the leading-edge, by the action of the VWE. This causes separation of the leading-edge and the flat surface, and allows continuous lubricant entry into the Hertzian zone, as well as the sideways flow divergence into the side-edges. With the increase in film-thickness due to the squeeze effect, and ultimately, solidification, in the side-edges, the load carrying duty is transferred to the side-edges. This ensures continued lubricant flow and separation of the ball and flat surface, until the lubricant exits the Hertzian zone, through the center and both side edges. This behaviour results in the horseshoe shaped deformation observed on the ball Hertzian zone, and on the disc, deformation occurs on the side-edges. The 150 N normal load is shared between the VWE and squeeze effect, and the VWE, being the dominant effect, carries a larger bulk of the normal load.

### *3.2.2 Role of the squeeze effect*

Since the effect of sliding speed on plastic deformation on the ball surface cannot be determined post the sliding process, from Fig. 4, it is assumed that during the downwards sliding motion of the ball surface, the change in sliding speed has negligible effect on the effective size of the ball Hertzian zone. Therefore, the width of the superimposed SLF shape does not change. On the contrary, the width of the Hertzian zone on flat surface, as observed previously, decreases at mid-stroke where the sliding speed is maximum ($W_{u_{max}}$) and increases at the top and bottom edges, where change in the sliding direction occurs and the sliding speed reaches a minimum ($W_{u_{min}}$). However, the width of the middle section ($W_B$) remains constant. Therefore, $W_B$ is not affected by the change in sliding speed, which indicates that the change in sliding speed only affects the flow behaviour on the side-edges. Following the downwards motion of the SLF, it can be seen that the decrease in the thickness of the side-edges is inwards, towards the middle section. Therefore, at the mid-stroke position, the Hertzian pressure transferred over a smaller area, positioned near the middle

section where the Hertzian pressure is higher on the flat surface. This behaviour is associated to the appearance of the squeeze effect due to the increase in the volume of lubricant entrained into the Hertzian zone at higher sliding speeds. Therefore, the change in sliding speed increases the squeeze effect and which affects the extent of solidification and Hertzian pressure transmission across the film-thickness. As a result, at maximum sliding speed ($W_{u_{max}}$), the film-thickness is larger, and higher Hertzian pressures are required for transfer across the larger film-thickness. From the deformation behaviour, is clear that such high pressures exist close to the middle section.

The action of the VWE is observable in the leading-edge of the ball surface, which aligns with the middle section of the flat surface during the sliding process. Since the change in sliding speed does not affect $W_B$, this suggests that the action of the VWE in the leading edge has no effect on the flat surface. Also, the VWE seems to have no effect in the side-edges. Therefore, the action of the VWE dominates in the leading-edge of the ball Hertzian zone, and the squeeze effect, dominates in the side-edges of both surfaces.

## 4 Summary

The appearance of the VWE in the leading-edge of the Hertzian zone creates collaboration with the squeeze effect, which appears and dominates in the side-edges. This collaboration results in the build-up and distribution of film pressure in the edges of the Hertzian zone on both the ball and flat surfaces, where the Hertzian pressure in low by convention. A schematic summary of the film-pressure distribution is shown in Fig. 7. This mechanism appears to be an efficient load carrying mechanism because the magnitude of the peak Hertzian pressure appears to be significantly lower, since the peak Hertzian pressure is spread and carried over a larger surface area, as opposed to being concentrated in a single point at the center of the Hertzian zone as per convention. These observations indicate that the appearance of a collaboration between the VWE and squeeze effect depends on the lubricant being in the fluid state, since the VWE and squeeze effect are fluid flow phenomenon. However, the build-up of film pressure by these two effects in their respective domains of action results in glass transition, and the appearance of the solid state of the lubricant, when the film pressure reaches $P_g$ of the lubricant. This phase transformation creates solid-to-solid conditions which cause the appearance of sliding fatigue wear (plastic deformation). Therefore, the VWE and the squeeze effect are primary mechanisms responsible for the build-up of film pressure, which increases the film thickness and keeps the sliding surfaces separated during the entire sliding process. Solidification becomes a secondary mechanism which takes over the load carrying duty and Hertzian pressure transfer duty from the VWE and squeeze effect, in their respective domains, when the film-pressure reaches $P_g$. The appearance of the VWE also indicates that temperature gradients large enough to induce the VWE appear in the leading edge on the ball surface. This is effect is associated to the curvature of the ball in the leading edge. The pressure generated by the VWE deforms the ball surface without affecting the flat surface, while the squeeze effect deforms both surfaces. The magnitude of the squeeze effect is offset by the increase in the sliding speed. It is not clear how this offset affects the load carrying capacity of the VWE in the leading edge. Further investigations are being done to uncover the effect of this offset. Fig. 8 shows the surface profiles obtained as illustrated in Fig. 7.

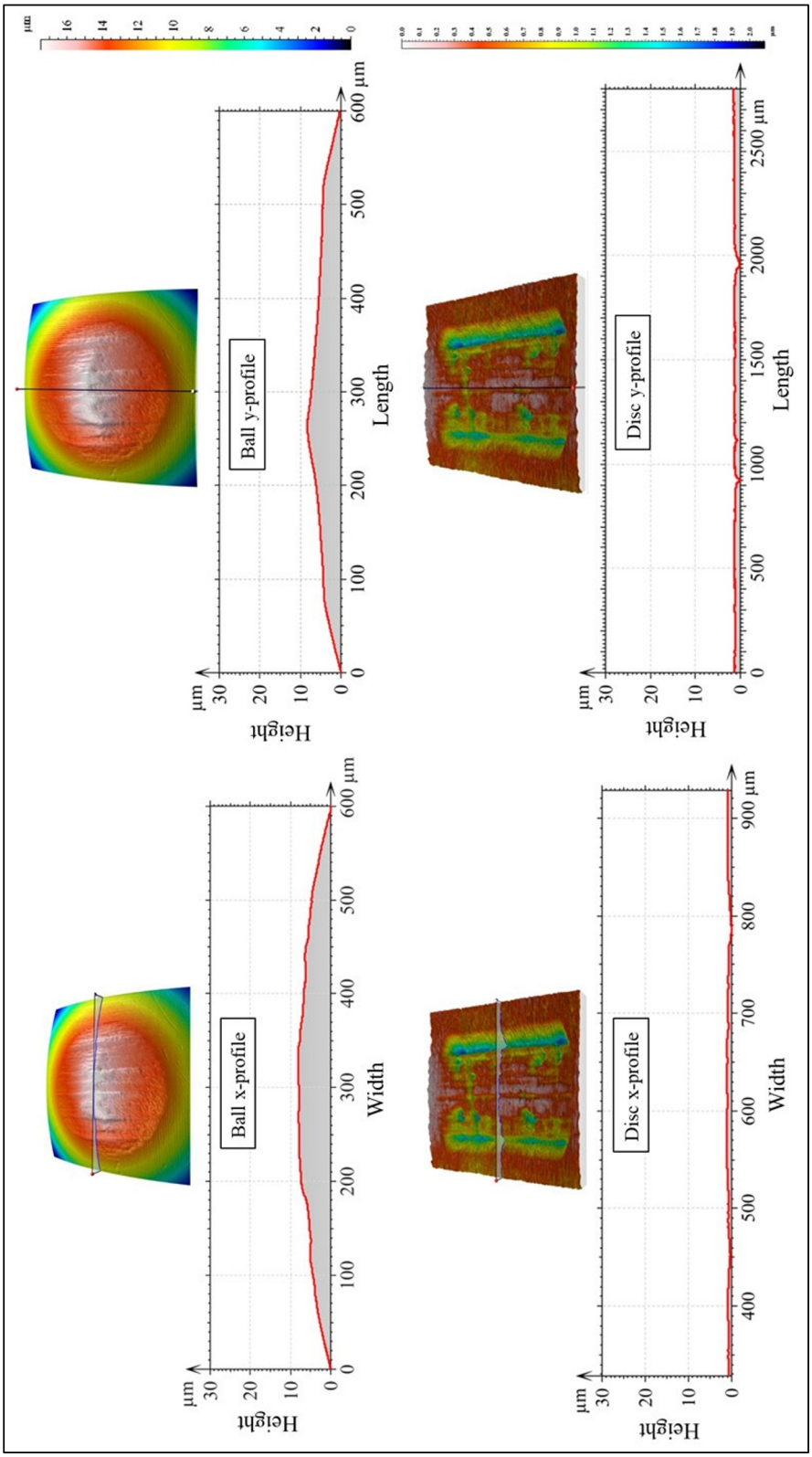


**Fig. 7.** Profiling of elastic deformation on ball and flat surfaces in the sliding direction (y-profile) and perpendicular to the sliding direction (x-profile).

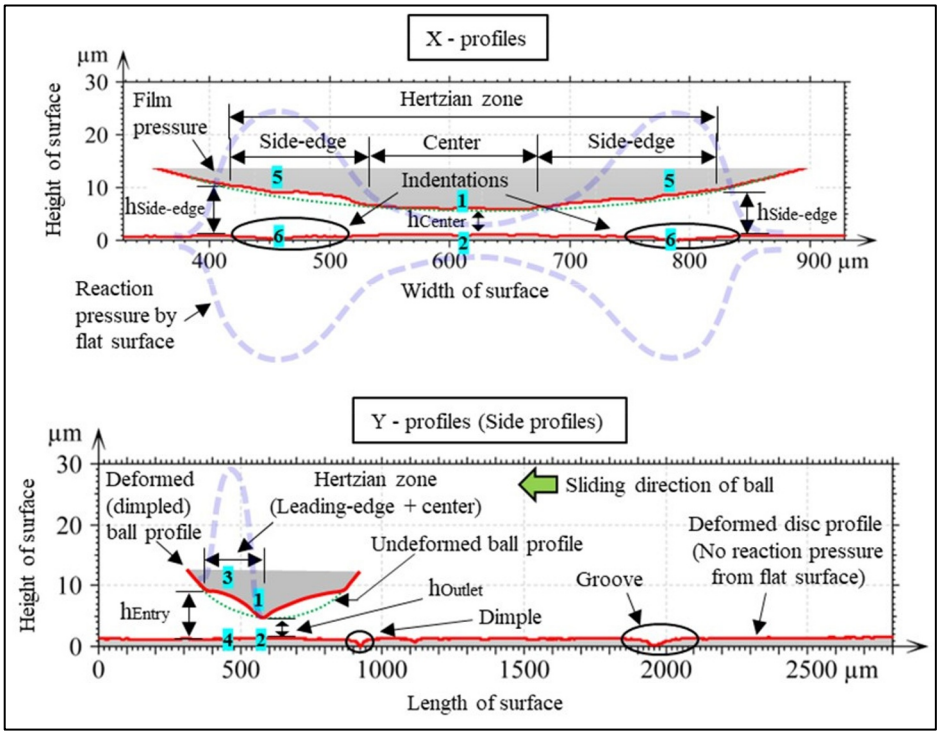


**Fig. 8.** Schematic summary of plastic deformation and film pressure behaviour in the Hertzian zone. X-profile – surface deformation across the center, perpendicular to sliding direction. Y-profile – surface deformation across the center, in the sliding direction.

The plastic deformation behaviour displayed on the deformed ball profile in Fig. 8 indicates that during the sliding process, the film-pressure at position 1 in the Hertzian zone is equivalent to that at position 2 (P1 ≈ P2). Furthermore, film-pressure at position 1 is less than that at position 3 (P1 << P3). Also, P3 >> P4, P4 ≈ P2, and P5 ≈ P6. The film-pressure is maximum in the edges of the Hertzian zone, where Hertzian pressure is minimal.

## 5 Conclusion

The appearance of a collaboration between the viscosity wedge effect (VWE) and the squeeze effect was demonstrated, for the first time, in a pure sliding AISI52100 ball bearing contact, through analysis of sliding contact fatigue and wear behaviour on the bearing surfaces. Surface analysis indicates the appearance of a horse-shoe shaped plastic deformation behaviour on the ball surface, which is dominated by a dimple shaped deformation in the leading-edge. On the flat surface, plastic deformation appears only in the side-edges. The center (middle section) of the Hertzian zones, on both surfaces, remain essentially undeformed. The deformation behaviour indicates that the film pressure is minimal at the center of the contact area, and maximum at the edges. The indicates an abnormal film-pressure distribution behaviour, since by convention in ball bearing contacts, the film pressure is maximum at the center, and minimum at the edges of the contact area. Therefore, the appearance of the VWE is described where dimple shaped surface deformation is observed, and the squeeze effect is described where deformation is influenced by the change in the sliding speed. This confirms the appearance of a collaboration between the two effects and reveals the domain of action of each effect on the ball and, for the first time, on the flat

surface. The dimple shaped deformation dominated the deformation behaviour, which indicates that the VWE dominated the film pressure generation during the operation of the bearing. The pressure generated by the VWE deforms the ball surface without affecting the flat surface, while the squeeze effect deforms both surfaces. Solidification of the lubricant explains the appearance of plastic deformation.

The authors would like to acknowledge the National Research Foundation (NRF) grant number: SFH170523232296, for financial support. The authorship contributions are: Sipho R. Masilela: Conceptualization, Methodology, Investigation, Validation, Writing - original draft & editing. Charles Siyasiya: Supervision, Validation, Writing - review & editing. Roelf Mostert: Supervision, Validation, Writing - review & editing.

## References

1. A. Gabelli, J. Lai, T. Lund, K. Rydén, I. Strandell, and G. E. Morales-Espejel, The fatigue limit of bearing steels – Part II: Characterization for life rating standards, Int. J. of Fatigue, vol. **38**, (2012). doi: https://doi.org/10.1016/j.ijfatigue.2011.12.006.
2. B. Meziane, N. Fillot, and G. E. Morales-Espejel, Synergy of Viscosity Wedge and Squeeze Under Zero Entrainment Velocity in EHL Contacts, Trib. Let., vol. **68**, 3 (2020). doi: 10.1007/s11249-020-01311-y.
3. E. Ciulli, T. Draexl, and K. Stadler, Film Thickness Analysis for EHL Contacts under Steady-State and Transient Conditions by Automatic Digital Image Processing, Adv. in Trib., vol. **2008**, (2008). doi: 10.1155/2008/325187.
4. A. Cameron, The Viscosity Wedge, A S L E Trans., vol. **1**, 2 (1958). doi: 10.1080/05698195808972337.
5. A. Fogg, Fluid Film Lubrication of Parallel Thrust Surfaces, Proc. of the Inst. of Mec. Eng., vol. **155**, 1 (1946). doi: 10.1243/pime_proc_1946_155_011_02.
6. J. A. Greenwood, Elastohydrodynamic Lubrication, Lubr., vol. **8**, 5 (2020). [Online]. Available: https://www.mdpi.com/2075-4442/8/5/51.
7. F. Guo and P. L. Wong, An Anomalous Elastohydrodynamic Lubrication Film: Inlet Dimple, J. of Trib., vol. **127**, 2 (2005). doi: 10.1115/1.1866165.
8. M. Omasta, I. Křupka, and M. Hartl, Effect of Sliding Direction on EHL Film Shape Under High Sliding Conditions, Trib. Trans., vol. **60**, 1 (2017). doi: 10.1080/10402004.2016.1147110.
9. X. M. Li, F. Guo, and P. L. Wong, Shear rate and pressure effects on boundary slippage in highly stressed contacts, Trib. Int., vol. **59**, (2013). doi: https://doi.org/10.1016/j.triboint.2012.06.030.
10. K. Yagi, K. Nishida, and J. Sugimura, Relationship between the molecular structure of lubricants and appearance of anomalous film shapes in elastohydrodynamic lubrication conditions, Trib. Int., vol. **152**, (2020). doi: https://doi.org/10.1016/j.triboint.2020.106574.
11. P. Wang and T. Reddyhoff, Wall slip in an EHL contact lubricated with 1-dodecanol, Trib. Int., vol. **113**, (2017). doi: https://doi.org/10.1016/j.triboint.2016.10.034.
12. P. L. Wong, X. M. Li, and F. Guo, Evidence of lubricant slip on steel surface in EHL contact, Trib. Int., vol. **61**, (2013). doi: https://doi.org/10.1016/j.triboint.2012.12.009.
13. A. Sarpal, M. Sastry, V. Bansal, I. Singh, S. Mazumdar, and B. Basu, Correlation of structure and properties of groups I to III base oils, Lub. Sci., vol. **24**, (2012). doi: 10.1002/ls.1172.
14. H. M. Kim and H. Spikes, Correlation of Elastohydrodynamic Friction with Molecular Structure of Highly Refined Hydrocarbon Base Oils, Trib. Let., vol. **68**, 1 (2020). doi: 10.1007/s11249-020-1265-5.

15. A. Alazizi, A. J. Barthel, N. D. Surdyka, J. Luo, and S. H. Kim, Vapors in the ambient—A complication in tribological studies or an engineering solution of tribological problems?, Fric., vol. **3**, 2 (2015). doi: 10.1007/s40544-015-0083-5.
16. X. Meng and M. M. Khonsari, On the effect of viscosity wedge in micro-textured parallel surfaces, Trib. Int., vol. **107**, (2017). doi: https://doi.org/10.1016/j.triboint.2016.11.007.
17. L. Paouris, R. Rahmani, S. Theodossiades, H. Rahnejat, G. Hunt, and W. Barton, An Analytical Approach for Prediction of Elastohydrodynamic Friction with Inlet Shear Heating and Starvation, Trib. Let., vol. **64**, 1 (2016). doi: 10.1007/s11249-016-0740-5.
18. H. Jamali, A. Al-Hamood, O. Abdullah, A. Senatore, and J. Schlattmann, Lubrication Analyses of Cam and Flat-Faced Follower, Lubr., vol. **7**, (2019). doi: 10.3390/lubricants7040031.
19. A. Bhattacharyya, G. Subhash, and N. Arakere, Evolution of subsurface plastic zone due to rolling contact fatigue of M-50 NiL case hardened bearing steel, Int. J. of Fatigue, vol. **59**, (2014). doi: https://doi.org/10.1016/j.ijfatigue.2013.09.010.
20. S. Bair, The viscosity at the glass transition of a liquid lubricant, Fric., vol. **7**, 1 (2019). doi: 10.1007/s40544-018-0210-1.
21. M. Tošić, R. Larsson, and T. Lohner, Thermal Effects in Slender EHL Contacts, Lubr., vol. **10**, 5 (2022). [Online]. Available: https://www.mdpi.com/2075-4442/10/5/89.